Nanoscale

PAPER

View Article Online
View Journal | View Issue

Cite this: *Nanoscale*, 2026, **18**, 3081

Chitosan conjugated cyclodextrin nanocomposite loaded with antibiotic-adjuvant combinations remediates multi-drug resistant *Staphylococcus aureus* infection in CD-1 mice model of bovine mastitis

Satwik Majumder,[a,b] Guillaume Millette,[c] Trisha Sackey,[b] Francois Malouin[c] and Saji George*[b]

Bovine mastitis (BM), resulting from intramammary infection, is one of the costliest diseases in animal agriculture. Occasional treatment failure and bacterial persistence in the mammary gland demand alternate therapeutic approaches. Nanotechnology-enabled Antibacterial Combination Therapy (NeACT), which utilizes nanomaterials to co-deliver more than one drug molecule with synergistic and complementary antibacterial mechanisms, holds promise for BM treatment. Here, we developed a NeACT constituting ceftiofur (CF) loaded chitosan nanoparticles conjugated with chlorpromazine (CPZ) and tannic acid (TA) loaded cyclodextrin nanoparticles. CF, CPZ, and TA showed a synergistic antibacterial action (FICI = 0.49) against a methicillin-resistant *Staphylococcus aureus* strain (Sa1158c) isolated from BM. NeACT demonstrated colloidal stability, biocompatibility, and slow-release of payloads and showed a significant reduction in Sa1158c efflux pump (by ~15.53-fold) and biofilm-forming (by ~3.40 $\log_{10}$) abilities. It showed low immunogenicity and no adverse effect on the mammary tissues of CD-1 lactating mice in a mastitis model. NeACT of ≥3.90 μg mL^{-1} demonstrated ≥3.20 $\log_{10}$ reduction of internalized Sa1158c in epithelial cells *in vitro*, while NeACT of 39 μg per gland showed ≥4.46 $\log_{10}$ remediation of Sa1158c from infected mice. Overall, NeACT successfully reduced the effective concentration of CF, CPZ, and TA and overcame Sa1158c CF resistance. These desirable therapeutic characteristics warrant its application for treating BM.

Received 11th September 2025,
Accepted 16th December 2025

DOI: 10.1039/d5nr03837e

rsc.li/nanoscale

1. Introduction

Bovine mastitis (BM) is the inflammation of the mammary gland tissues, primarily resulting from an intramammary infection (IMI).[1] Owing to reduced milk production, milk loss, treatment failures, *etc.*, the yearly financial loss in some prominent milk-producing countries such as the United States, Canada, and India amounts to $2 billion, $310 million, and $971 million, respectively, making BM the most threatening bacterial disease in the dairy cattle industry.[1] Out of several contagious pathogens, *Staphylococcus aureus* is one of the most prevalent organisms associated with BM, accounting for almost 40–70% of the cases globally.[2] *S. aureus* colonizes tissues lining the milk-collecting spaces and induces weak inflammation and host immune responses.[1] This ability in *S. aureus* is predominant in their persistence and chronic infection.[1]

The treatment of BM often involves intramammary infusion or parental administration of antibiotics to dairy cows during lactation or the dry period.[1] According to the United States Department of Agriculture (USDA), cephalosporins (53.2%), lincosamide (19.4%), and non-cephalosporin β-lactam antibiotics (19.1%) are the most common antibiotics in use to treat BM.[3] Non-selective blanket antimicrobials used as prophylactic control often impart selective pressure on mastitis pathogens such as *S. aureus*, leading to antimicrobial resistance (AMR).[4] Such pathogens may possess intrinsic or acquired resistance mechanisms that could limit drug uptake, inactivate/modify a drug, and show virulence, such as biofilm formation, hemolysin production, intracellular survivability,

[a]*Environmental and Occupational Health Sciences Institute (EOHSI) and School of Public Health, Rutgers University, Piscataway, NJ 08854, USA. E-mail: satwik.majumder@rutgers.edu*
[b]*Department of Food Science and Agricultural Chemistry, Macdonald Campus, McGill University, 21, 111 Lakeshore Ste Anne de Bellevue, Quebec H9X 3 V9, Canada. E-mail: trisha.sackey@mail.mcgill.ca, saji.george@mcgill.ca; Tel: (+1) 514-398-7920*
[c]*Département de biologie, Faculté des sciences, Université de Sherbrooke, Sherbrooke, Quebec J1K 2R1, Canada. E-mail: guillaume.millette@USherbrooke.ca, francois.malouin@USherbrooke.ca*

etc., contributing to treatment failures.[5–7] Indeed, the cure rate of *S. aureus*-mediated mastitis in cows with intramammary treatment during lactation or at dry-off rarely exceeds 50%.[8] The prevalence of AMR among mastitis pathogens is rising, evidenced by the increasing resistance rate towards crucial antibiotics such as beta-lactams and cephalosporins, between 30–70% in the USA and more than 85% in Ireland and Brazil.[9] Vaccines against S. *aureus in* BM, namely Lysigin® in the USA and Startvac® in Europe and Canada, failed to provide significant protection against reinfection.[10,11] Overall, these challenges warrant cost-effective, sustainable alternate strategies that are efficient in BM treatment.

Antibacterial combination therapy is defined as '*combining antibiotic/s and/or adjuvant molecules with synergistic properties to improve antibacterial treatment outcomes*'.[1] The mechanism of such a combination involves common or complementary interactions, including sequential inhibition of the same biochemical pathway, inhibition of bacterial antimicrobial-modifying enzymes, *etc.*[12–14] Although combination therapy has been employed in biomedical and agricultural sectors, poor drug bioavailability, retention rate, cytotoxicity, stability, and overdosing have restricted its widespread acceptance.[1] We believe that nanotechnology-enabled approaches could resolve these issues. The nano size and multifunctionality of nanomaterials provide unprecedented advantages for the targeted delivery of drugs across biological barriers.[1,15] We term this strategy as Nano-enabled Antibacterial Combination Therapy (NeACT) and define it as '*the therapeutic strategy aimed at harnessing the power of a nano-delivery platform to deliver more than one drug molecule with complementary function for effective antibacterial treatment*'.[1]

In this study, we selected ceftiofur (CF), a cephalosporin, as the primary antibiotic for combination therapy. Although CF is extensively used in subclinical BM, it could have a cure rate as low as 0% against *S. aureus*.[8,16,17] Chlorpromazine (CPZ) and a polyphenol, Tannic acid (TA), were selected as adjuvants as they complement the action of CF by inhibiting bacterial efflux pumps, disrupting biofilms and membrane integrity.[18–20] Chitosan (CH) is a polysaccharide widely used in nanomedicine because of its desirable characteristics for drug delivery, such as cationic charge, biocompatibility, low toxicity, low immunogenicity, ability to adhere to mucosal surfaces, and improved permeability of macromolecules through the epithelial tight junction.[21] CH nanoparticles have been reported to exhibit prolonged residence time at drug absorption sites, enabling higher drug penetration and targeting intracellular pathogens, thus being suitable as a single drug carrier in complex IMI environments, meriting their application as a carrier for CF.[21] The hydroxypropyl derivatives of β-cyclodextrin (CD) are biocompatible cyclic oligosaccharides containing a relatively hydrophobic central cavity and hydrophilic outer surface.[22] CD has been reported to improve solubility and enhance drug stability, drug molecule permeability, and bioavailability.[22] It can encapsulate or adsorb multiple payloads due to its hydrophobic central cavity and hydrophilic outer surface. Therefore, we selected CD as a carrier for CPZ and TA. Overall, we designed a unique nanocomposite constituting CF-loaded CH nanoparticles conjugated with CPZ and TA-loaded CD nanoparticles (hereafter referred to as NeACT). NeACT was tested under an *in vitro* system to understand its mechanism of action against pathogens. Further, its ability to remediate an IMI caused by a methicillin-resistant *Staphylococcus aureus* strain isolated from BM was verified successfully using the lactating CD-1 mouse mastitis model.

2. Materials and methods

2.1. Reagents and chemicals

The (2-hydroxypropyl)-β-cyclodextrin (CD) (molecular weight: ~1396 Da) (product number: H107), chitosan (85% deacetylated) (CH) (medium molecular weight) (product numher: 448877), tannic acid (TA) (molecular weight: 1701.20) (product number: 16201), chlorpromazine (CPZ) (molecular weight: 355.33) (product number: C8138), ceftiofur (CF) (molecular weight: 523.56) (product number: 34001), sodium tripolyphosphate (TPP), Mueller–Hinton Broth (MHB), dimethyl sulfoxide (DMSO), resazurin sodium salt, nylon filter membranes (of 0.22 μm and 0.45 μm), insulin, hydrocortisone, poly-L-lysine, fluorescein isothiocyanate (FITC), glutaraldehyde solution, and ethidium bromide (EtBr) were purchased from Sigma-Aldrich, Canada. The 32-gauge blunt needles were purchased from TSK Laboratory International, Canada. Gibco Dulbecco's Modified Eagle's medium (DMEM), Hoechst 33342, propidium iodide (PI), Probe–On Plus slides, and Sterile Petri dishes were purchased from ThermoFisher, Canada. Fetal bovine serum (FBS) was purchased from Wisent, Canada. Gentamicin sulfate was purchased from Bio Basic, Canada. Human colorectal adenocarcinoma (Caco-2) cells were purchased from ATCC, USA. The quality control (QC) strain *Staphylococcus aureus* ATCC 25923 was purchased from Oxoid Company, Canada. The methicillin-resistant *S. aureus* strains Sa1158c (Isolate ID: 10812464, Accession no. NCBI: SRR11471981) and Sa30 (Isolate ID: 21000024, Accession no. NCBI: JAANBF000000000) were collected from the Canadian mastitis pathogen culture collection (MPCC).[7] CD-1 lactating mice were purchased from Charles River Laboratories, Canada.

2.2. Assessment of CF, CPZ, and TA for antibacterial synergism

A three-dimensional checkerboard assay, as previously described by Stein *et al.*, was conducted to assess the antibacterial efficiency of the combination (CF, TA, and CPZ).[23] More information on the checkerboard assay is provided in SI 1.

2.3. Synthesis of CPZ and TA-loaded CD nanoparticles (CPZ-CD-TA)

A 6 : 6 : 6 mM ratio of CD, TA, and CPZ was used for CPZ-CD-TA preparation. Briefly, 138.6 mg of CD was dispersed in 3 mL of ethanol and sonicated for 10 min. The resulting suspension was added dropwise to a solution of CPZ (28.62 mg) in 10 mL of DI water under constant stirring.

CPZ-CD was sonicated for 15 min, and a 2 mL ethanol solution containing 153.09 mg of TA was added dropwise. CPZ-CD-TA was kept under constant stirring for 5 hours at 40 °C and then under vacuum for 30 min. Subsequently, the solution was filtered using a 0.45 μm nylon filter membrane to remove the unreacted agents and residual impurities. CPZ-CD-TA was refrigerated at −20 °C and lyophilized using a freeze dryer (FreeZone 12L-50C, Labconco Corp., USA). The dried sample was stored in a desiccator for future use.

2.4. Synthesis of CPZ-CD-TA conjugated CF-loaded CH nanoparticles (CH Np-CF(CPZ-CD-TA) or NeACT)

CH (2 mg mL^{-1}) was added to DI water, dissolved by adding acetic acid (final concentration of 1%), and stirring the solution for 48 h. Subsequently, the pH was raised to 4.7–4.8 using 1 N NaOH. CF (1.5 mg mL^{-1}) was dissolved in DI water and added to the CH solution dropwise. The resulting mixture was stirred for 15 min and sonicated for another 15 min. TPP, at a concentration of $1/3^{rd}$ of CH, was added dropwise to the solution under constant stirring to form CH Nps entrapping CF. The formed CH Np-CF was stirred for 30 min, sonicated for 15 min, and stirred for another 1 h. The sample was centrifuged (7500*g* for 10 min) (Sorvall Instruments, Thermo Fisher Scientific, USA), washed, and resuspended in PBS. Freeze-dried CPZ-CD-TA was added to the PBS buffer and dispersed with sonication and vigorous stirring. CH Np-CF was added dropwise to the solution at a 3 : 1 ratio (CPZ-CD-TA : CH Np-CF) and stirred for 4 h to allow fusion between the two entities through electrostatic interaction. The CH Np-CF(CPZ-CD-TA), referred to as NeACT, was washed thrice, resuspended in PBS, and stored at 4 °C for further analysis.

2.5. Fluorescein isothiocyanate (FITC) labeling of NeACT

As-synthesized NeACT (10 mg mL^{-1}) was added to FITC (1 mg mL^{-1}, dissolved in DMSO) at room temperature and incubated under vigorous stirring in the dark for 12 h. The FITC-labeled NeACT (FITC-NeACT) was centrifuged (7500*g* for 10 min) and washed thoroughly with sterile DI water until no color or residue was observed in the supernatant. Fluorescence images of particles were taken using an automated *epi*-fluorescence microscope (Cell Discoverer 7, Carl Zeiss, Germany) to confirm the labeling of NeACT with FITC.

2.6. Physicochemical characterization of the particles

Attenuated total reflectance-Fourier transform infrared (ATR-FT-IR), Scanning Electron Microscope (SEM), and Dynamic Light Scattering (DLS) analysis were used to assess the surface functional groups, surface morphology, and hydrodynamic size and surface charge of the particles, respectively. More information on the physicochemical characterization of the particles is provided in SI 2.

2.7. Loading capacity of particles and release profile of CF, CPZ, and TA

The loading capacity of the particles and release profile of the drug molecules (CPZ, TA, and CF) were determined using a Varian ProStar HPLC system (Varian, USA) equipped with a Gemini-NX 5u C18 110A column (100 × 4.60 mm, 5 μm particle size, Phenomenex, USA). For this, NeACT particles (1 mg mL^{-1}) were centrifuged (31 000*g* for 20 min) (Sigma 3–30 KHS, Germany), as centrifugation at high RPM could disrupt the polymeric matrix to release the contents.[24] The supernatants were filtered using a 0.22 μm nylon filter membrane. A 20 μL of the supernatant was injected into the chromatographic system. The mobile phase consisted of methanol–acetonitrile-acetic acid (5%) in a volume ratio of 6 : 7 : 87 at a 1.2 mL min^{-1} flow rate. The detection wavelengths for CPZ, TA, and CF were 306 nm, 280 nm, and 292 nm, respectively. The availability (amount of payload contained by nanocarrier) of CPZ, TA, and CF in NeACT was subsequently determined from a standard curve (concentration range: 1 mg mL^{-1}–0.05 mg mL^{-1}).

The loading capacity was determined following eqn (1).

$$\%\ \text{Loading capacity} = (\text{concentration of 'X' in supernatant after centrifuging NeACT/initial concentration of 'X' added during the synthesis of NeACT}) \times 100 \quad (1)$$

where 'X' is CF, CPZ, or TA.

To determine the release profiles of CPZ, TA, and CPZ from NeACT as a function of time, a 1 mg mL^{-1} NeACT suspension was prepared in 10 mL of PBS buffer, supplemented with 10% FBS (pH 7.4) to mimic the bovine mammary microenvironment. The suspension was incubated at 37 °C under minimal shaking at 100 rpm. One milliliter of NeACT was gently centrifuged (3000*g* for 1 min), and the supernatant was collected every 24 hours for a period of seven days. The supernatant was filtered, and the HPLC was used to quantify CF, CPZ, and TA in the supernatant as detailed above. The percentage of payload release as a function of time was determined following eqn (2).

$$\%\ \text{Payload release} = (\text{concentration of 'X' in supernatant each day of sample collection/initial concentration of 'X' in NeACT}) \times 100 \quad (2)$$

where 'X' is CF, CPZ, or TA.

2.8. *In vitro* antibacterial efficiency of particles

The *in vitro* antibacterial efficiency of the particles was determined using a broth microdilution method.[25] More information on this method is provided in SI 3.

The effect of particles on bacterial membrane integrity was assessed using a PI dye uptake assay.[12] As detailed earlier, the particles (125 μg mL^{-1}) were subjected to ten-twofold serial dilution in 100 μL of MHB media in a 96-well plate. Ten μL of the culture maintained at a 0.5 McFarland standard was added to the wells and incubated for 6 h at 37 °C. PI dye (3.34 μg mL^{-1}) suspended in PBS was added to the wells and incubated for 30 min. The fluorescence intensity was measured at an

excitation/emission wavelength of 555/645 nm using a plate reader (SpectraMax-i3X, Molecular devices, USA) to assess PI uptake into cells with compromised membranes.

SEM was used to assess changes in the morphological features of bacteria after being exposed to NeACT.[26] Briefly, bacterial culture maintained at 0.5 McFarland standard was subjected to a sub-lethal concentration (1.95 μg mL^{-1} or half of the MIC value against Sa1158c) of NeACT and incubated for 6 h at 37 °C with gentle shaking. Bacterial cells were harvested by centrifugation (4000*g*, 3 min) and washed twice with PBS (1×, pH 7.4). The washed cells were fixed using 2.5% glutaraldehyde at 4 °C for 2 h. Fixed cells were dropped onto poly-L-lysine-coated coverslips and subjected to serial dehydration by exposing them to incremental concentrations of ethanol (20–100%). Further, these cells were subjected to critical point drying (Leica EM CPD300, Germany) and were used for SEM examination after sputter coating with Platinum. ImageJ software was used to measure the size of bacterial cells.

2.9. Efficiency of NeACT against resistance mechanisms of *S. aureus*

The anti-efflux activity of NeACT was measured using a pre-established EtBr assay.[14] Briefly, bacterial cultures maintained at 1.0 McFarland standard (3×10^8 cells per mL) were treated with sub-lethal concentrations ($1/3^{rd}$ of MIC value against Sa1158c) of NeACT (1.30 μg mL^{-1}) and control groups (CH Np-CF (20.83 μg mL^{-1}) and CPZ-CD-TA (83.33 μg mL^{-1})). The suspension was vortexed and incubated at 37 °C for 30 min. A sub-lethal concentration of EtBr (0.65 μg mL^{-1} or $1/3^{rd}$ of the MIC value against Sa1158c) was added further to the suspension and incubated for another 30 min. Bacterial cells were washed, re-suspended in PBS (1×, pH 7.4), and transferred (140 μL) to a 96-well plate. EtBr efflux was triggered by glucose (10 μL; final concentration 0.1% w/v), and efflux activity was determined by monitoring the increase in fluorescence intensity (530/590 nm) for 60 min using a plate reader. Sa1158c, without particle exposure, was considered a positive control, while Sa25923, with no efflux pump activity, was used as a negative control. GraphPad Prism 7 software was used to determine the time-dependent efflux of EtBr using a single exponential decay equation, as detailed previously.[6] The time taken for the bacterial cells to extrude 50% of EtBr was denoted as $t_{efflux50\%}$.

For assessing the antibiofilm property of NeACT,[12] 200 μL of TSB media suspended with incremental concentrations (0.24–125 μg mL^{-1}) of NeACT and control particles in a 96-well plate were added with 20 μL of the Sa1158c culture adjusted to 0.5 McFarland standard. After 48 h of incubation, the media were removed from the wells, and the wells were washed with sterile PBS. Subsequently, 100 μL of 99% methanol was added, and the plates were kept undisturbed for 15 min. Methanol was removed from the wells, and 200 μL of CV solution (0.4%) was added. The plates were incubated for 2 h, washed, and 100 μL of acetic acid (33%) was added. The biomass of the biofilms was quantified by measuring the absorbance values at 570 nm using a plate reader.

The viability of Sa1158c cells present in biofilm was assessed after treating with increasing concentrations (0.24–125 μg mL^{-1}) of the particles. Briefly, 10 μL of the Sa1158c isolate maintained at a 0.5 McFarland standard was added to 100 μL of TSB media in a 96-well plate. The plate was incubated for 24 h to allow biofilm formation, followed by the addition of NeACT and control particles. The plate was incubated for another 24 h at 37 °C. The 100 μL of TSB media was discarded without damaging the biofilm. Subsequently, 100 μL of PBS was added to the wells containing biofilms, and the biofilm cells were suspended by vigorous pipetting. The CFU was enumerated using the drop plate culturing method, as detailed in SI 3.

To visualize the penetration of NeACT into the biofilm matrix, a fluorescent-labeled Sa30 isolate was obtained by introducing plasmid pSRFPS1 (coding red fluorescence protein (RFP)) [7] was used. Ten μL of RFP labeled Sa30 isolate (maintained at 0.5 McFarland standard) was incubated for 24 h (at 37 °C) in a 96-well plate containing 100 μL of TSB media to allow biofilm formation. FITC-NeACT (20.83 μg mL^{-1} or $1/3^{rd}$ of the MIC value against Sa30) was exposed to the biofilms and incubated further for 24 h. Subsequently, 100 μL of the TSB media was discarded, and 100 μL of PBS was added to the wells. Fluorescence images of the biofilms (Red fluorescence imaged using a 583 nm filter) and FITC-NeACT (Green fluorescence imaged using a 519 nm filter) were captured at 20× magnification using an epifluorescence high content microscope (Cell Discoverer 7). 3D images were constructed by stacking images captured from different depths.

2.10. Efficiency of NeACT against internalized *S. aureus* in epithelial cells

The cytotoxicity of NeACT was tested in Caco-2 cells. The efficiency of NeACT in targeting internalized *S. aureus* in epithelial cells (Caco-2) was also determined. More information on the method is provided in SI 4.

2.11. Efficiency of NeACT in a murine model of mastitis

The institutional ethics committee on animal experimentation of the Faculté des Sciences of the Université de Sherbrooke (QC, Canada) approved the *in vivo* experiments, and the guidelines of the Canadian Council on Animal Care were respected during all procedures.

CD-1 lactating mice were separated from their pups (12–14 days following birth) and anesthetized using isoflurane.[27] The fourth pair of glands, found from head to tail (L4 and R4 glands), was first disinfected with 70% ethanol for inoculation. A 100 μL of PBS containing 100–125 CFUs of Sa1158c was slowly injected into the lactiferous duct with a 32-gauge blunt needle attached to a 1 mL syringe. Four hours post-inoculation, mice were anesthetized again, and incremental concentrations of NeACT (20 (78 μg per gland), 10 (39 μg per gland), and 5 (19.5 μg per gland) times of *in vitro* MIC value against Sa1158c) were injected directly into the previously infected mammary glands (6 mammary glands: $n = 6$). Similarly, CH Np, CD, CH Np-CF, and CPZ-CD-TA (working

concentration: 78 μg per gland or 20 times of *in vitro* NeACT MIC value against Sa1158c) were used as control particles and were injected into the infected mammary glands (6 mammary glands per control group). Hundred μL of PBS used as the media control was injected into eight infected mammary glands (n = 8). Each infected gland was considered as an experimental unit. After 14 h of bacterial inoculation, mice were anesthetized and humanely euthanized, mammary glands were harvested, and one set was homogenized for measuring bacterial count; the other set was kept for histological studies (see section 2.12). CFU counts were obtained after plating a serial dilution of mammary gland homogenates on TSA Petri dishes that were incubated at 37 °C for 24 h. The detection limit was approximately 200 CFU per gram of mammary glands.

2.12. Tissue preparation and histological studies

Mammary glands from the NeACT-treated and untreated mice were fixed in 4% PFA overnight at 4 °C, dehydrated in 70% ethanol to avoid adipose distortion, and embedded in paraffin.[28] Subsequently, the paraffin blocks were incubated at −20 °C for 1 h. Tissue sections of 5 μm were cut using a microtome (Shandon Finesse ME + paraffin sectioning microtome, GMI, USA), applied to Probe–On Plus slides, and kept at room temperature. Hematoxylin and Eosin Y (H&E) staining and Masson's trichrome staining were performed to investigate immune responses and morphological and cellular alterations in infected and NeACT-treated mammary glands, while Gram staining was performed to stain and detect Sa1158c in infected mammary tissues. H&E and Masson's trichrome staining was conducted on an automated platform (Shandon varistain 24-4 slide stainer, GMI, USA). Tissue preparation, embedding, and coloration (H&E, Masson's trichrome, and Gram staining) were performed by the Electron Microscopy and histology platform at the Université de Sherbrooke.[27] Images were captured on a Nanozoomer Digital Slides Scanner (Hamamatsu, Japan).

2.13. Statistical analysis

t-Test and one-way ANOVA were performed as required to check the statistical significance, wherein a p-value ≤ 0.05 was considered significant. 'GraphPad Prism 7' software was used to perform the statistical analysis.

3. Results

3.1. Checkerboard assay

The checkerboard assay assessed the combinatorial effect of the CF, CPZ, and TA against Sa1158c. An FICI of <0.8 was considered a synergistic relationship among the combinations. The MICs of CF, CPZ, and TA against Sa1158c were 31.25, 500, and 500 μg mL^{-1}, respectively. Notably, the CLSI breakpoint for CF is ≥8 μg mL^{-1}, suggesting CF resistance by Sa1158c. When CF, CPZ, and TA were combined, the MICs were reduced significantly by 8-fold (MIC: 3.91 μg mL^{-1}), 4-fold (MIC: 125 μg mL^{-1}), and 8-fold (MIC: 62.5 μg mL^{-1}), respectively. The FICI for combinations of CF, CPZ, and TA was 0.49, indicating a synergistic interaction.

3.2. Physicochemical characterization of the particles

The FTIR spectra of NeACT is provided in Fig. 1a. In NeACT, CH Np-CF was evident from the peaks at 2938 and 2892 cm^{-1} (stretching vibrations of methylene groups), 1065 cm^{-1} (C–O–C stretching vibrations), 1526 cm^{-1} (–NH_2 bending vibration peak), 1026 cm^{-1} (P═O stretching vibration), 1759 cm^{-1} (C═O stretching), 1382 cm^{-1} (C–N stretching), and 1690 cm^{-1} (thioester group). The signals at 859 cm^{-1} (α-type glycosidic bond),

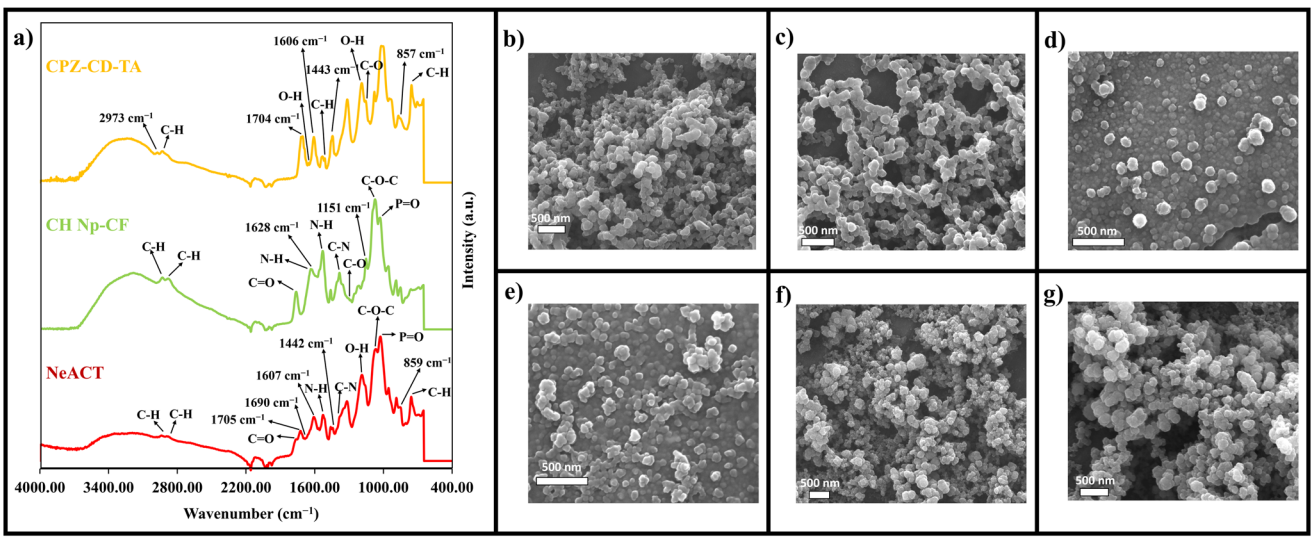

Fig. 1 Physicochemical characterization of the particles. (a) FT-IR analysis of the particles analyzed at a wavelength range of 600–4000 cm^{-1} with a resolution of 4 cm^{-1}. Scanning electron microscopy (SEM) images of (b) CD-NP, (c) CPZD-CD-TA, (d) CH Np, (e) CH CF-Np, (f and g) NeACT. The particles were dropped onto aluminium mounts, dried, and coated with platinum. The images were acquired using an SEM.

2938 cm^{-1} (C–H stretching vibration), 1187 cm^{-1} (O–H bending), 1442–1705 cm^{-1} (benzene rings), 1607 cm^{-1} (phenyl rings), 756 cm^{-1} (aromatic C–H bending) corresponded to the functional groups of CPZ-CD-TA in NeACT. The shifts in FTIR spectra in the case of NeACT indicate hydrogen bonding formation due to the interactions between the payloads and the nanocarriers. More details on the functional groups associated with CPZ-CD-TA and CH Np-CF are provided in SI 2.

SEM analysis revealed the morphology of the particles (Fig. 1b–g). CPZ-CD-TA conjugated with CH Np-CF through electrostatic interactions to develop NeACT and ranged between ~250–400 nm. The hydrodynamic sizes of CH Np, CH Np-CF, and NeACT were ~269, ~309, and ~539 nm, respectively. The zeta potential for CH Np and CH Np-CF ranged between +28–30 mV, which, however, reduced to ~+21.6 mV in the case of NeACT, indicating the electrostatic interaction between CH Np-CF and CPZ-CD-TA (Table 1). Indeed, a zeta potential close to +30 mV suggests sufficient repulsive forces and superior physical colloidal stability.[12] More information on the SEM and DLS analysis associated with CD Np, CH Np, CPZ-CD-TA, and CH Np-CF is provided in SI 2.

Table 1 The hydrodynamic size and zeta potential of the particles

Samples	Hydrodynamic size (nm)	Zeta potential (mV)
CD Np	137.41 ± 5.91	−11.37 ± 1.37
CH Np	269.56 ± 3.43	+29.89 ± 0.62
CH Np-CF	309.52 ± 5.11	+30.68 ± 1.21
CPZ-CD-TA	132.77 ± 4.84	−9.51 ± 1.56
NeACT	539.58 ± 12.36	+21.69 ± 2.43

3.3. Loading capacity of NeACT and release profile of CF, CPZ, and TA

The loading capacity of NeACT for the payloads was determined using HPLC. The availability (amount of payload contained in nanocarrier) of CF, CPZ, and TA in 1 mg mL^{-1} of NeACT was ~32.14%, ~18.78%, and ~16.85%, respectively (Fig. 2a). The availability of CF in 1 mg mL^{-1} of CH CF-Np was 44.66%, while the loading capacity of CD Np (1 mg mL^{-1}) for CPZ and TA were 26.88% and 25.78%, respectively. The release profile of NeACT was monitored every 24 h for 7 days in PBS buffer supplemented with 10% FBS (pH 7.4). The release of 50% CF, CPZ, and TA from 1 mg mL^{-1} of NeACT was observed between the 2nd and 3rd day, while a 100% release was seen by the 7th day (Fig. 2b).

3.4. *In vitro* antibacterial efficiency and mechanism of action of NeACT

NeACT showed excellent antibacterial properties against the tested bacteria, Sa1158c and Sa25923. For instance, the MIC for NeACT against Sa25923 and Sa1158c were 0.48 μg mL^{-1} and 3.91 μg mL^{-1}, respectively. NeACT showed a ~7.05 $\log_{10}$ Sa25923 reduction and ~7.51 $\log_{10}$ Sa1158c reduction ($p < 0.05$) at the MIC (Fig. 3a and b). On the contrary, CF, CPZ, TA, CPZ-CD-TA, and CH Np-CF at the same concentrations showed no significant difference ($p > 0.05$) from the control group (Sa25923 and Sa1158c without treatment). The MIC for CPZ-CD-TA and CH CF-Np against Sa1158c was 250 and 62.5 μg mL^{-1}, respectively. The MICs for pristine CF, CPZ, and TA were 31.25, >250, and >250 μg mL^{-1}, respectively, against Sa1158c. Interestingly, the availability of CF, CPZ, and TA in NeACT at its MIC (3.91 μg mL^{-1}) against Sa1158c was 1.25,

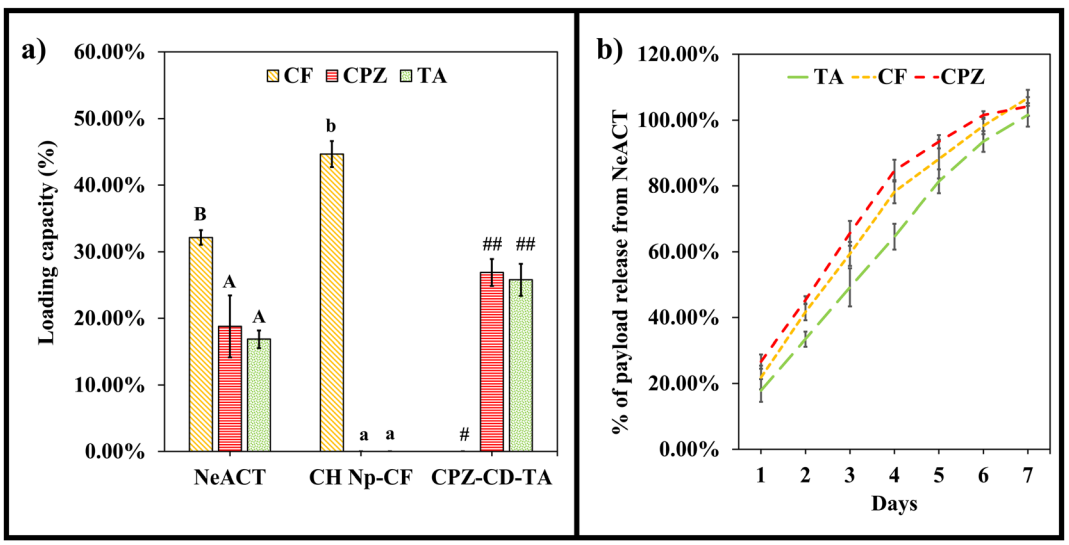

Fig. 2 Loading capacity of particles and release profile of the payloads. (a) The loading capacity of the particles for CF, CPZ, and TA. The particles of 1 mg mL^{-1} were centrifuged and filtered. An HPLC system was used to assess the availability of CPZ, TA, and CF in the particles. (b) The release profile of CF, CPZ, and TA from NeACT. The release of CF, CPZ, and TA was checked every 24 h for seven days. NeACT of 1 mg mL^{-1} was centrifuged gently, and the supernatant was collected. HPLC was used to assess the percentage of payload release. Average values plotted in the graph with different alphabets and symbols indicate a significant difference ($p < 0.05$).

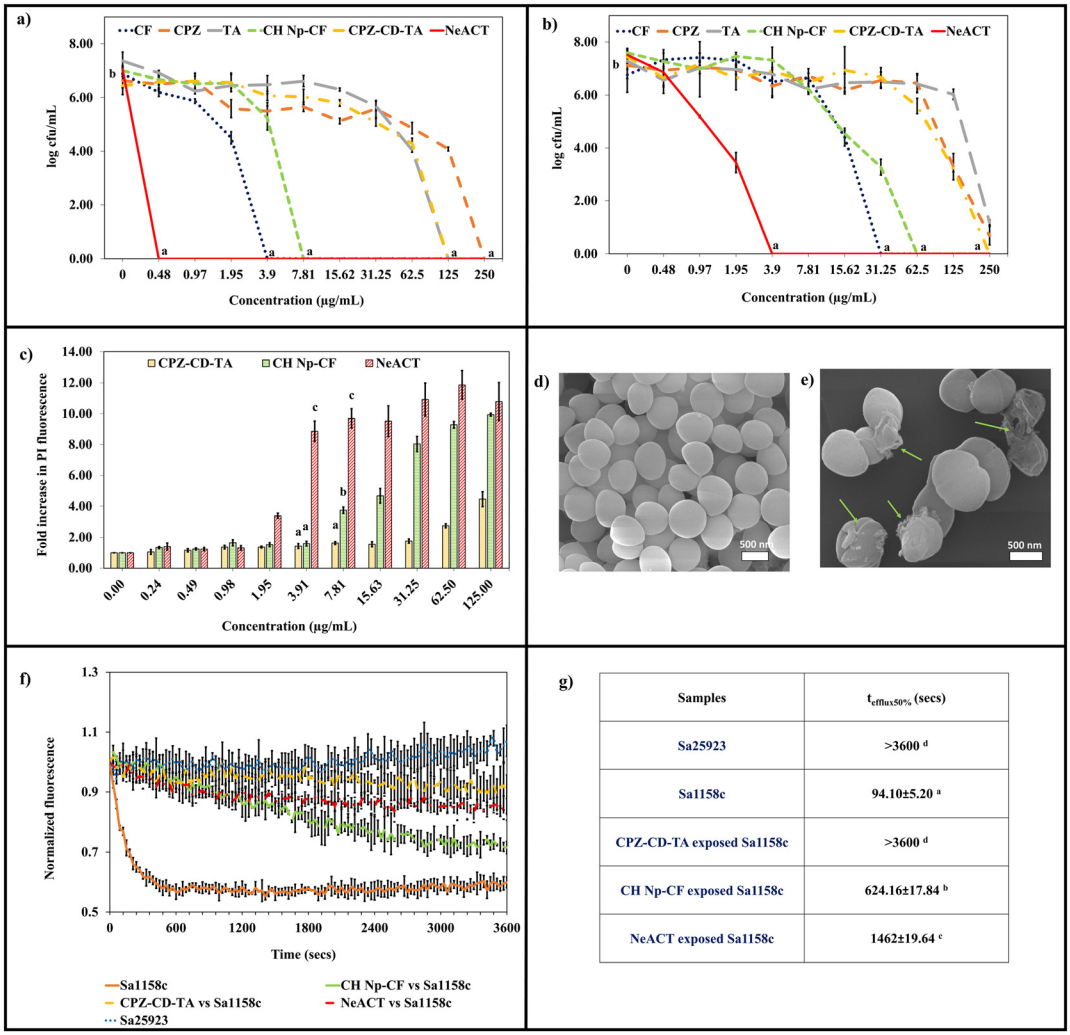

Samples	$t_{efflux50\%}$ (secs)
Sa25923	>3600 ^{d}
Sa1158c	94.10±5.20 ^{a}
CPZ-CD-TA exposed Sa1158c	>3600 ^{d}
CH Np-CF exposed Sa1158c	624.16±17.84 ^{b}
NeACT exposed Sa1158c	1462±19.64 ^{c}

Fig. 3 Antibacterial efficiency and mechanism of action of particles against *S. aureus*. (a and b) Antibacterial efficacy of NeACT and control groups against (a) Sa25923 and (b) Sa1158c. In a 96-well plate, the incremental concentration of the samples was subjected to MHB media containing bacteria maintained at 0.5 McFarland standard. The plate was incubated for 18 h, and the CFU was enumerated using the drop plate culturing method. (c) Sa1158c membrane integrity upon particle exposure. After 6 h of incubation, PI dye was added to the wells. The fluorescence intensity was measured at an excitation/emission wavelength of 555/645 nm using a plate reader. Average values plotted in the graph with different alphabets indicate a significant difference ($p < 0.05$). (d and e) SEM image of (d) untreated Sa1158c cells and (e) NeACT-treated Sa1158c cells. Bacterial cells were exposed to sub-lethal concentrations of NeACT for 6 h. The cells were harvested, washed, and fixed with 2.5% glutaraldehyde. Critical point drying was performed, and the cells were coated with platinum and examined under SEM. Green arrows indicate compromised membrane integrity. (f and g) Efflux pump inhibition property of the particles. Sa1158c culture was subjected to a sub-lethal concentration of the particles followed by a sub-lethal dosage of EtBr. The cells were harvested, washed, and transferred to a 96-well plate. Glucose was added, and EtBr efflux was monitored at an excitation/emission wavelength of 530/590 nm using a plate reader. A single exponential decay equation was used to determine the time-dependent efflux of EtBr. The time taken by the cells to extrude 50% of the EtBr was denoted as $t_{efflux50\%}$. Average values plotted in the table and graph with different alphabets indicate a significant difference ($p < 0.05$).

0.73, and 0.65 µg mL^{-1}, respectively (based on the loading capacity of NeACT), suggesting a significant decrease in the effective concentration of CF (by 25-fold), CPZ (by >342-fold), and TA (by >384-fold) than their pristine form. This superior performance of NeACT was owed to the synergistic effect of the combination.

The effect of NeACT on bacterial membrane integrity was measured by PI uptake assay (Fig. 3c). NeACT showed significant damage to the Sa1158c membrane. For instance, at 3.91 µg mL^{-1}, a ~8.85-fold increase ($p < 0.05$) in PI fluorescence was observed, suggesting a compromised Sa1158c membrane. The rate of damage increased with increasing concentrations of NeACT. Compared to the control group (bacteria with no treatment), CPZ-CD-TA at 62.5 µg mL^{-1} and CH Np-CF at 31.25 µg mL^{-1} showed ~2.74 and ~8.03-fold increase in PI fluorescence, respectively. Fig. 3d and e represent Sa1158c cells before and after exposure to 1.95 µg mL^{-1} of NeACT. Ruptured membrane and corrugated morphology with wrin-

kles and cracks were evident in NeACT-treated Sa1158c cells due to the loss of membrane integrity.[29]

Sa1158c cells extruded 50% of the EtBr molecules ($t_{efflux50\%}$) in only 94.10 s, while the exposure (1/3rd of MIC value against Sa1158c) of CPZ-CD-TA (at 83.33 μg mL^{-1}), CH Np-CF (at 20.83 μg mL^{-1}), and NeACT (at 1.30 μg mL^{-1}) reduced the extrusion rate significantly ($p < 0.05$) by >38.25-fold, ~6.63, and ~15.53-fold, respectively, suggesting the efflux inhibition property of the particles (Fig. 3f and g). It was evident that CPZ-CD-TA has contributed to the efflux inhibition property in NeACT.

The ability of NeACT to restrict biofilm formation was verified (Fig. 4a). CPZ-CD-TA, CH Np-CF, and NeACT inhibited 50% biofilm formation at 9.73, 69.14, and 0.45 μg mL^{-1}, respectively. While CPZ-CD-TA reduced Sa1158c biofilms by ~3.18 $\log_{10}$ at 125 μg mL^{-1}, NeACT (at 3.91 μg mL^{-1}), and CH Np-CF (at 62.5 μg mL^{-1}) showed ~3.38 $\log_{10}$ and ~3.70 $\log_{10}$ reduction, respectively (Fig. 4b). To investigate the penetration and accumulation of FITC-labelled NeACT (coding green), a sub-lethal dosage (20.83 μg mL^{-1} or 1/3rd of FITC-NeACT MIC value against Sa30) was subjected to the biofilms of RFP-tagged Sa30 (coding red). Compared to untreated control, a significant reduction in biofilm biomass was evident (Fig. 4c–f). Moreover, Z-stack images suggested the accumulation and penetration of NeACT in Sa30 biofilms (Fig. 4e and f).

3.5. Efficiency of NeACT against internalized *S. aureus* in epithelial cells

The efficiency of NeACT against internalized pathogens was examined in a Caco-2 cell model of intracellular infection, where the Caco-2 cell line was used as a representative model epithelial cell line. No cytotoxicity was detected for the tested particles (NeACT, CH CF-Np, CPZ-CD-TA, CH Np, and CD Np) in Caco-2 cells, as 100% viability was observed at 250 μg mL^{-1} of the particles (Fig. 5a) (the highest dose tested). NeACT showed a significant reduction in intracellular Sa1158c (Fig. 5b). For instance, at the MIC value of 3.9 μg mL^{-1}, NeACT showed a 3.27 $\log_{10}$ reduction ($p < 0.05$) of internalized Sa1158c from the Caco-2 cells. Similarly, at 7.81 and 15.62 μg mL^{-1}, NeACT reduced intracellular Sa1158c colonization by 4.49 $\log_{10}$ and 7.01 $\log_{10}$, respectively.

3.6. *In vivo* efficiency of NeACT on CD-1 mice model of mastitis infection

CD-1 lactating mice were used as a mastitis infection model to evaluate NeACT efficiency. A 7.4 $\log_{10}$ Sa1158c CFU g^{-1} of tissue was detected from mammary glands without treatment (Fig. 5c). As expected, CPZ-CD-TA had no effect on Sa1158c inhibition, while CH Np-CF (at 78 μg per gland) showed a significant ~3.44 $\log_{10}$ Sa1158 reduction. NeACT showed a superior ($p < 0.05$) remediation of Sa1158c from the mammary gland compared to all control groups. For instance, a low dose of 78 μg per gland and 39 μg per gland of NeACT showed ~5.13 $\log_{10}$ (>99.999%) and ~4.46 $\log_{10}$ (>99.99%) Sa1158c reduction, respectively, from mice mammary gland.

H&E and Masson's trichrome staining were performed on mammary tissues to examine PMN infiltration, morphological, and cellular alterations. No inflammation and negligible PMN infiltration (as the large dark purple spheres with a multilobular nucleus, indicated with black arrows in Fig. 6a–d) or lesions in the supportive connective tissue were observed in the untreated noninfected tissues and NeACT-treated noninfected tissues. Adipocytes (indicated with red arrows in Fig. 6a–h) were evident in all the tissues as signet-shaped cells, with a nucleus at the periphery, with visible fat droplets, and a thin layer of cytoplasm. The pink staining within the alveoli represented milk components.[30] Compared to NeACT-treated infected tissues, collapsed alveoli and necrotic areas were detected in untreated infected tissues. Moreover, PMN infiltration (indicated with black arrows in Fig. 6e–h) was significantly evident in the connective tissue and intraluminal space of the untreated infected tissues.

4. Discussion

We designed and tested a novel Nano-enabled Antibacterial Combination Therapy (NeACT) comprised of ceftiofur (CF)-loaded chitosan nanoparticles (CH Np) conjugated with chlorpromazine (CPZ) and tannic acid (TA)-loaded cyclodextrin nanoparticles (CD Np). NeACT demonstrated exceptional colloidal stability, biocompatibility, and slow-release properties of the payloads. The synergistic interaction of components used in NeACT resulted in a dramatic decrease in bacterial load in a mouse model of mastitis.

Previously, our group reported the characterization of a library of *S. aureus* strains isolated from bovine mastitis for antibiotic resistance and virulence traits.[7] In that study, we identified Sa1158c as an MDR MRSA strain resistant to CF (the antibiotic used in this study).[7] Studies have reported that the cure rate of MDR *S. aureus* infection by CF could be around 47% but could get as low as 0%.[8,16,17] As anticipated, we observed a synergistic action among CF, CPZ, and TA. This is ascribed to the complementary mode of action of the selected antibiotic-adjuvant combination (as discussed later).

We examined the release profile of CF, CPZ, and TA from NeACT every 24 h for seven days. A 50% release of all the payloads was observed within 2–3 days. The release of CPZ and TA from CD Np is probably through dilution-mediated dissociation,[31] while the release of CF from CH Np is probably through diffusion or shrinkage, causing release due to attractive electrostatic interaction between anions and chitosan matrix at a higher pH.[32,33] Compared to previous studies that reported a much faster release of drugs (within 6 to 12 h) from polymeric nanoparticles,[32] our observations suggested a slow-release behavior of payloads from the nanocarriers. One of the most significant drawbacks of CF is its elimination before 12 h after intramammary infusion, as it gets rapidly metabolized.[34] The slow release of payloads from NeACT could contribute significantly to improving the retention time of CF in the mastitis microenvironment.

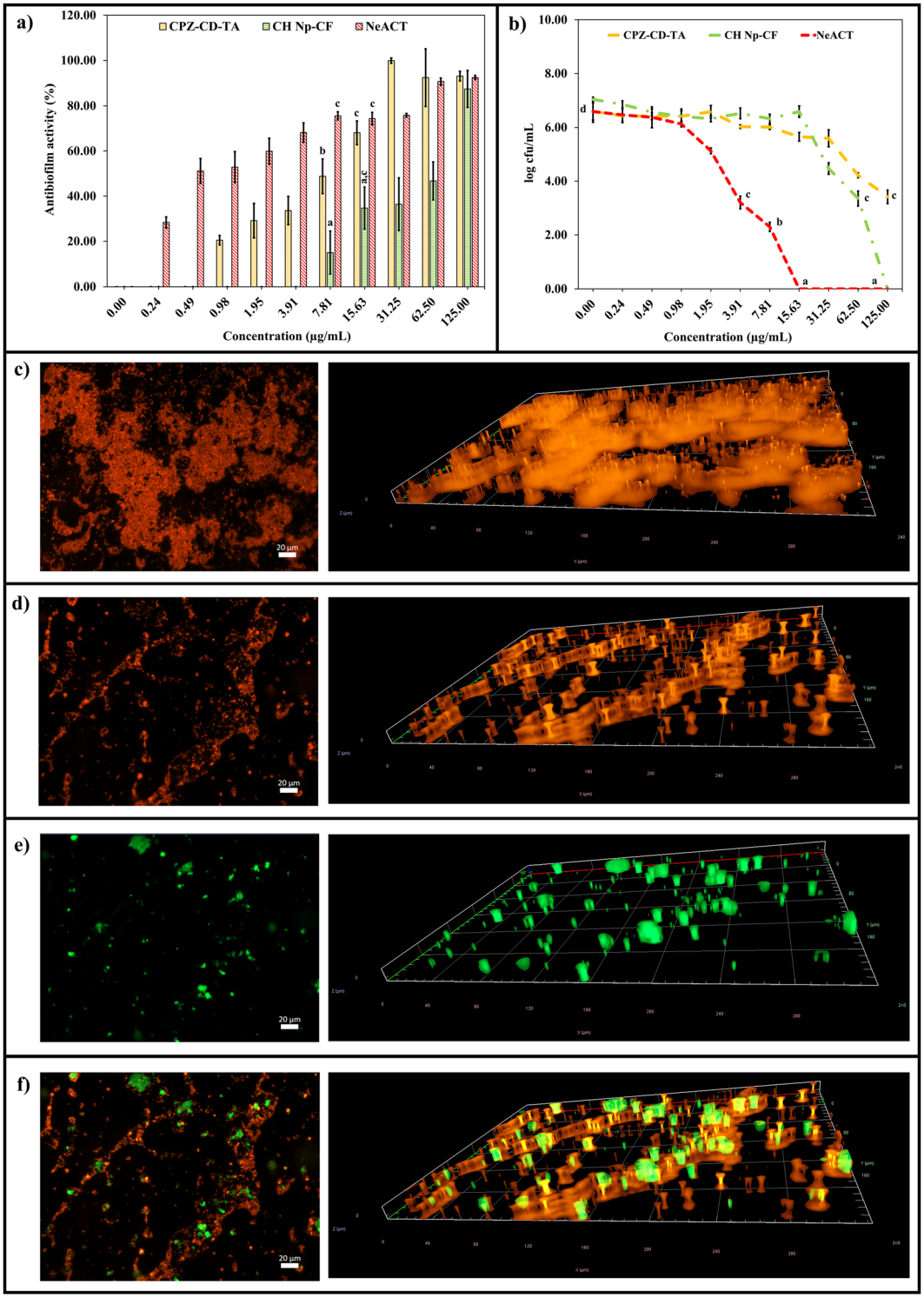

Fig. 4 Mechanism of action of the particles against *S. aureus* biofilms. (a) Antibiofilm activity of the particles. Incremental concentrations of the particles were suspended in TSB media containing Sa1158c culture. After 48 h of incubation, the media was removed, 99% methanol was added, wells were washed gently, and resuspended with CV solution. The plates were incubated for 2 h, washed, and acetic acid (33%) was added. The biofilm biomass was quantified by measuring the absorbance at 570 nm. (b) Inhibition of matured biofilms by the particles. Matured biofilms formed after 24 h of incubation were exposed to incremental concentration of the particle in a 96-well plate. The plate was incubated for 24 h. The biofilms were collected, and the CFU was enumerated using the drop plate culturing method. Average values plotted in the graph with different alphabets indicate a significant difference ($p < 0.05$). (c–f) Epifluorescence and *Z*-stack images of (c) untreated RFP-tagged Sa30 biofilms, (d) treated RFP-tagged Sa30 biofilms, (e) FITC-NeACT signal in Sa30 biofilms, and (f) overlapped signals of FITC-NeACT penetrating RFP tagged Sa30 biofilms. A sub-lethal dosage of FITC-NeACT was exposed to matured biofilms of RFP-tagged SA30. Cell Discoverer 7 was used to capture *epi*-fluorescence images of the biofilms (coding red at 583 nm) and FITC NeACT (coding green at 519 nm). *Z*-Stack images of different layers were constructed.

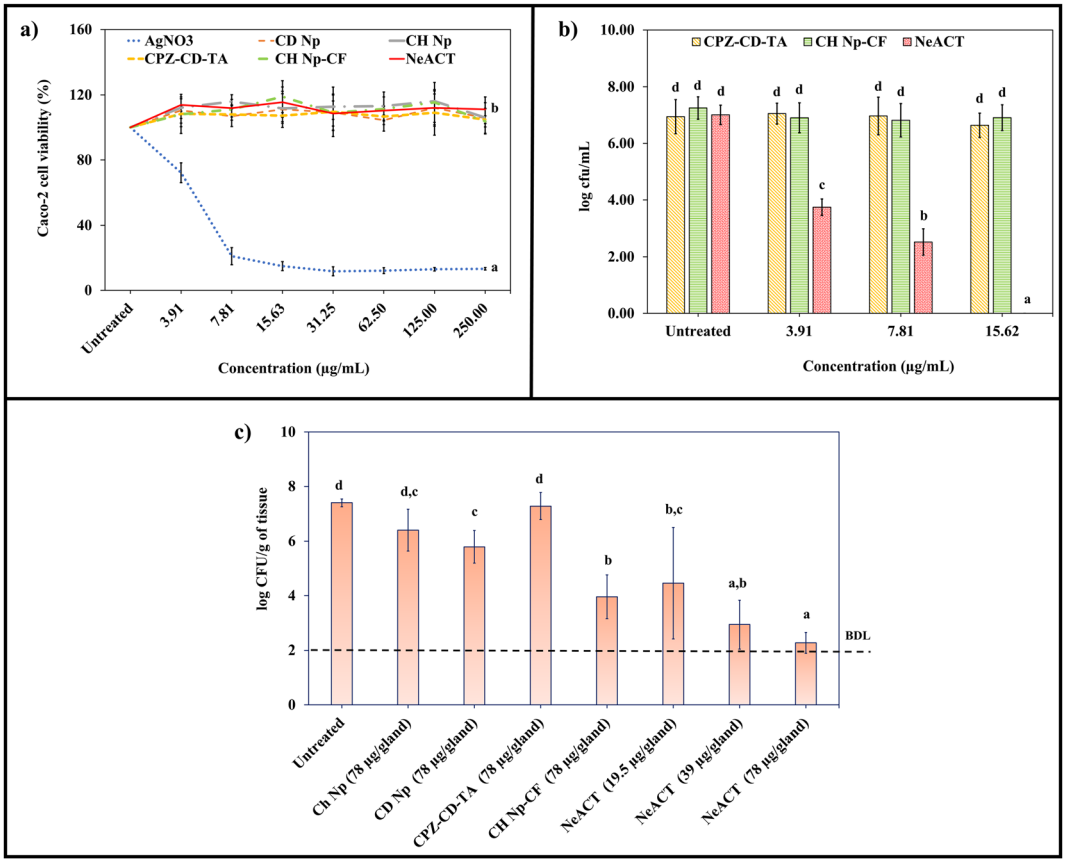

Fig. 5 Cytoxicological assessment and intracellular infection remediation study in Caco-2 cells and *in vivo* efficiency of the particles in infected CD-1 lactating mice model. (a) Cytotoxicity of the particles in Caco-2 cells. Confluent cells (2×10^4 cells per well) were exposed to an incremental concentration of the particles in DMEM media in a 96-well plate. After 24 h of incubation, resazurin was added to the wells, and the plate was incubated for 4 h further. Fluorescence intensity was measured at 530/590 (excitation/emission). (b) Intracellular Sa1158c remediation efficiency of the particles. Confluent Caco-2 cells were exposed to Sa1158c culture and incubated in a 96-well plate for an hour. The cells were washed, subjected to gentamicin, and incubated for 30 min. The extracellular gentamicin was washed, and the plate was incubated with DMEM for 4 h. Incremental concentrations of the particles were added to the wells and incubated for 24 h. Further, the cells were washed and lysed using Triton X. Drop culture method was used for CFU enumeration of viable intracellular Sa1158c. Average values plotted in the graph with different alphabets indicate a significant difference ($p < 0.05$). (c) Sa1158c infection remediation efficiency of the particles from CD-1 lactating mice mammary glands. Sa1158c of 100–125 CFUs were injected into the lactiferous duct of CD-1 lactating mice. Certain concentrations of the particles were directly injected into the mammary glands previously infected. After 14 h of incubation, mice were humanely euthanized, and mammary glands were harvested and homogenized. CFU counts were obtained from mammary gland homogenates on TSA plates. The detection limit was approximately 200 CFU g^{-1} of mammary glands. Average values plotted in the graph with different alphabets indicate a significant difference ($p < 0.05$).

NeACT showed excellent antibacterial efficiency *in vitro* against Sa1158c at a dosage of 3.9 µg mL^{-1}. Based on the loading capacity of NeACT, the amounts of CF, CPZ, and TA contained in 3.91 µg mL^{-1} of NeACT were 1.25, 0.73, and 0.65 µg mL^{-1}, respectively. Previous studies from our group reported that Sa1158c possesses efflux pump activity, beta-lactamase enzyme production, and strong biofilm-forming ability.[7] Genomic studies revealed genes associated with major facilitator superfamily (MFS) efflux pumps (*norA*, *norB*, *tetM*, *etc.*), cephalosporin resistance (*blal*, *blaR*, *blaZ*, *mecA*, *etc.*), and fibronectin-binding proteins (*fnbA*, *fnbB*, *etc.*), underpinning efflux activities.[7] Therefore, the efficiency of NeACT was tested against these resistance mechanisms. The increase in PI fluorescence suggested that NeACT disrupted the Sa1158c cell membrane. Interestingly, a significant increase in width was noticed among the Sa1158c cells under NeACT stress. Cell wall-targeting antibiotics, such as CF, bind to penicillin-binding proteins (PBPs) and inhibit peptidoglycan synthesis, thereby affecting septal cell wall synthesis and forming wider cells with a lower surface-to-volume ratio.[35] A sub-lethal dose (1.30 µg mL^{-1}) of NeACT significantly inhibited Sa1158c efflux. The penetration of antimicrobials into the dense protective layer of biofilms is crucial for their eradication. NeACT was highly effective in restricting biofilm growth and inhibiting mature biofilms by accumulating and penetrating the biofilm layer.

The superior efficiency of NeACT against such resistance mechanisms of Sa1158c is ascribed to the complementary mode of action of the antibiotic-adjuvant combinations. CF is considered bactericidal as it binds to PBPs and interferes with

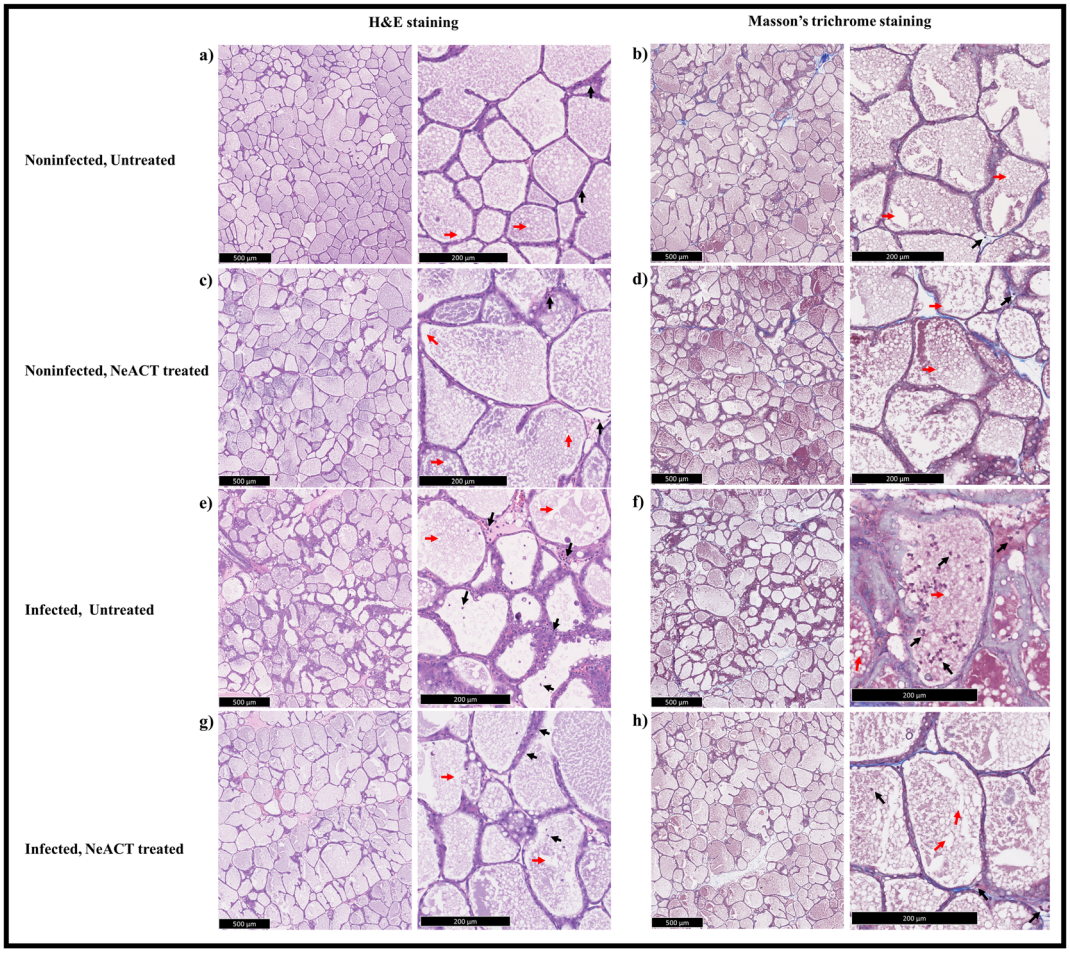

Fig. 6 Histopathological analysis of CD-1 mice mammary tissue. (a) H&E staining and (b) Masson's trichome staining of noninfected and untreated mammary tissue. (c) H&E staining and (d) Masson's trichome staining of noninfected but NeACT-treated mammary tissue. (e) H&E staining and (f) Masson's trichome staining of infected but untreated mammary tissue. (g) H&E staining and (h) Masson's trichome staining of infected and NeACT-treated mammary tissue. The mammary glands were fixed in 4% PFA, dehydrated, and embedded in paraffin. Tissue preparation, embedding, and coloration were performed by the Electron Microscopy and histology platform at the Université de Sherbrooke. The black and red arrows denote the PMN infiltration and adipocytes, respectively.

cell wall enzymes, leading to cell lysis and death. Although CPZ and TA are not known to inhibit bacterial growth at low dosages, they contribute significantly to anti-efflux and anti-biofilm properties, as observed in this study. TA is a strong electron donor that interferes with the hydrolysis of ATP, causing an increase in bacterial membrane permeability and thus enabling the passage of NeACT through the cell wall.[18] The free phenolic hydroxyl groups in TA affect bacterial enzymatic activity *via* covalent or non-covalent linking.[18] Moreover, TA has been reported to disrupt peptidoglycan formation, iron chelation, and fatty acid synthesis.[18] CPZ complements the effect of TA and CF by crippling the function of specific drug-resistance transporters and multidrug MFS efflux pumps and exhibiting conformational changes in efflux protein structures.[36,37] CPZ has also been reported to interact with several membrane-active proteins, including FtsA and FabI, and exhibit strong anti-biofilm action.[19] Moreover, CPZ has been reported to disrupt the sensor-inducer protein of the *S. aureus* cell membrane and suppress *bla* and *mec* gene expression, which play a predominant role in producing resistance factors such as PBP2a and β-lactamase.[20] Additionally, chitosan-loaded CPZ exhibited antibiofilm activity.

One of the prominent virulence characteristics that enables *S. aureus* to persist in mammary tissue is its ability to invade and reside as an intracellular pathogen.[7] Therefore, we checked the efficiency of NeACT in combating intracellular Sa1158c in Caco-2 cells. NeACT showed no cytotoxicity and excellent remediation of intracellular Sa1158c. Earlier, our groups reported that pristine CF and CPZ were marginally effective against intracellular pathogens.[7,14] As such, the superior outcome observed in NeACT can be attributed to the combined impact of the drug molecules and the favourable interaction and absorption of NeACT by the Caco-2 cells. To ensure efficient cell interaction and intracellular transmission of a nanoparticulate system, a positive zeta potential, such as that observed in NeACT, is crucial.[38] Previous studies have

shown that the endocytic uptake of CH Np is significantly influenced by clathrin-mediated translocation.[39] CD Np undergoes macropinocytosis as the primary uptake mechanism in Caco-2 cells.[40] It's likely that NeACT utilizes a sequential release mechanism for its payloads. According to Zaki *et al.*, delivering a high initial dose of antimicrobials inside cells, followed by a sustained antibiotic release, could be an effective approach for treating intracellular infections. This method reduces relapses and ensures efficient treatment.[41]

Clinical trials conducted in animals have revealed that nearly 30% of drug candidates identified from preclinical screening fail due to toxic effects, while 60% do not deliver the desired results.[42] This underscores the significance of exploring the efficacy of NeACT in treating BM using *in vivo* models. Intraductal CD-1 lactating mice have been shown to accurately replicate *S. aureus*-induced bovine mastitis, thereby serving as a valuable adjunct for *in vivo* research.[27,43] NeACT demonstrated excellent remediation of Sa1158c infection by ~5.13 $\log_{10}$ and ~4.46 $\log_{10}$ in the CD-1 mice mammary gland at a dosage of 78 and 39 μg per gland, respectively. Based on the loading capacity of NeACT, the amounts of CF, CPZ, and TA contained in 39 μg per gland of NeACT were 12.53, 7.32, and 6.57 μg per gland, respectively. Histopathological examination suggested that the exposure to NeACT neither induces inflammation nor impacts cell and tissue morphology. An excessive amount of cell infiltration, along with classical immune cell activation, was observed in infected mouse mammary glands, which led to tissue damage. Meanwhile, a minimal inflammatory cell infiltration, as observed in NeACT-treated and infected mammary glands, is a crucial element in the healing process. While the antibacterial effect of NeACT could be explained by the combined action of CF and effector molecules, the components of NeACT could also influence the tissue response to infection. Several studies have demonstrated the potential anti-inflammatory and wound-healing properties of TA.[44,45] The exact mechanism through which TA exerts these effects is not yet fully understood. However, scientific reports suggest that TA may stimulate healing by modulating growth factors and activating the extracellular signal-regulated kinase 1/2 (ERK1/2) pathway.[44] Previous research has demonstrated that CH exerts anti-inflammatory effects by modulating macrophage polarization from the pro-inflammatory M1 to the anti-inflammatory M2 state.[46] In addition, it promotes an immune response that leads to the secretion of anti-inflammatory mediators, such as the interleukin-1 receptor antagonist (IL-1ra) and interleukin-10 (IL-10).[46] Previously, the CD was found to effectively decrease the concentration of various pro-inflammatory cytokines, including interleukin-1 alpha (IL-1α), tumor necrosis factor (TNF), and interleukin-6 (IL-6).[47] All in all, our studies suggest that the design and choice of drug components are suitable for ameliorating intramammary infection. The nanometric dimensions and surface chemistry are thought to facilitate the penetration of NeACT into the tissue matrix (and bacterial biofilm, if present), and the release of effective concentrations of antibiotics and effector molecules in the vicinity of bacterial cells to eliminate the infection.

5. Conclusion

BM caused by microbial infections is one of the costliest diseases in the dairy industry worldwide. The failure of conventional treatment and management strategies demands alternative approaches. Nano-enabled Antibacterial Combination Therapy (NeACT) that harnesses the potential of nano-delivery platforms for antibiotic/adjuvant combination of synergistic functions holds promise in effective BM treatment. In this study, a NeACT was developed, consisting of CF-loaded CH Np conjugated with CPZ and TA-loaded CD Np. NeACT demonstrated exceptional stability, biocompatibility, slow-release behavior of payloads for efficient delivery, and successfully remediated intracellular and intramammary infections of multi-drug-resistant MRSA. Future clinical studies are needed to assess the efficacy, safety, and tolerability of NeACT in treating mastitis in cattle. The fate of NeACT after achieving its therapeutic goals in the bovine mammary gland requires extensive study. This includes evaluating the NeACT degradation, metabolism, and impact on the host and the environment. As evidenced by our study, the slow-release behaviour of payloads from nanocarriers can prolong their persistence in mammary tissue, thereby increasing the risk of NeACT residues in milk, which in turn interferes with dairy processing and poses human health concerns. Therefore, rigorous studies on the withdrawal period of NeACT are mandatory to ensure milk safety, regulatory compliance, and consumer protection.

Author contributions

Satwik Majumder: nanomaterial synthesis and characterization, *in vitro* studies, data curation, formal analysis, investigation, methodology, validation, visualization, writing – original draft & editing. Guillaume Millette: *in vivo* study, histology, data curation, formal analysis, methodology, validation, visualization. Trisha Sackey: *in vitro* studies, formal analysis, methodology, validation. Francois Malouin: funding acquisition, methodology, resources, supervision, validation. Saji George: conceptualization, funding acquisition, investigation, project administration, methodology, resources, supervision, validation, review & editing manuscript.

Conflicts of interest

The authors (Satwik Majumder, Guillaume Millette, Trisha Sackey, Francois Malouin, and Saji George) declare that they have no known competing financial interests or personal relationships that could have appeared to influence the work reported in this paper.

Data availability

The data supporting the findings of this study are provided in the paper and supplementary information (SI). Supplementary information is available. See DOI: https://doi.org/10.1039/d5nr03837e.

Acknowledgements

The authors acknowledge funding CRC/George/X-coded/248475 and CFI 254248 for supporting this research work. This work was also supported by a team grant (no. 328798) from the Fonds de Recherche du Québec – Nature et Technologie (FRQ-NT) to S. G. and F. M., and we acknowledge support from Op + lait, Regroupement stratégique FRQ-NT, pour un lait de qualité optimale (Université de Montréal, St-Hyacinthe, QC, Canada). The authors thank Dr Jennifer Ronholm, McGill University, for providing the *Staphylococcus aureus* 1158c (Isolate ID: 10812464) and Sa30 (Isolate ID: 21000024) isolates. The authors thank the Facility for Electron Microscopy Research (FEMR) and the Multiscale Imaging Facility, McGill University. The authors thank the Histology and electron microscopy platform of Université de Sherbrooke. S. M. acknowledges student aid from the McGill Graduate Excellence Award, and G. M. received an Alexandre-Graham-Bell doctoral research studentship from the Natural Sciences and Engineering Research Council of Canada and a studentship from FRQ-NT during this study.

References

1 S. Majumder, P. D. Eckersall and S. George, *ACS Agric. Sci. Technol.*, 2023, **3**, 562–582.
2 W. N. Cheng and S. G. Han, *Asian-Australas. J. Anim. Sci.*, 2020, **33**, 1699–1713.
3 O. Kerro Dego, Bovine Mastitis: Part I, in *Animal Reproduction in Veterinary Medicine*, ed. F. Aral, R. Payan-Carreira and M. Quaresma, IntechOpen, 2021, ch. 8, DOI: 10.5772/intechopen.93483.
4 G. Normanno, G. La Salandra, A. Dambrosio, N. Quaglia, M. Corrente, A. Parisi, G. Santagada, A. Firinu, E. Crisetti and G. Celano, *Int. J. Food Microbiol.*, 2007, **115**, 290–296.
5 J.-H. Fairbrother, S. Dufour, J. M. Fairbrother, D. Francoz, É. Nadeau and S. Messier, *Vet. Microbiol.*, 2015, **176**, 126–133.
6 S. Majumder, D. Jung, J. Ronholm and S. George, *BMC Microbiol.*, 2021, **21**, 222.
7 S. Majumder, T. Sackey, C. Viau, S. Park, J. Xia, J. Ronholm and S. George, *BMC Microbiol.*, 2023, **23**, 43.
8 O. K. Dego and J. Vidlund, *Front. Vet. Sci.*, 2024, **11**, 1356259.
9 H. Barkema, Y. Schukken and R. Zadoks, *J. Dairy Sci.*, 2006, **89**, 1877–1895.
10 A. J. Bradley, J. E. Breen, B. Payne, V. White and M. J. Green, *J. Dairy Sci.*, 2015, **98**, 1706–1720.
11 J. R. Middleton, J. Ma, C. L. Rinehart, V. N. Taylor, C. D. Luby and B. J. Steevens, *J. Dairy Res.*, 2006, **73**, 10–19.
12 S. Majumder, C. Viau, A. Brar, J. Xia and S. George, *Appl. Clay Sci.*, 2022, **228**, 106569.
13 S. Majumder, J. Zhou and S. George, *LWT*, 2024, **210**, 116842.
14 A. Brar, S. Majumder, M. Z. Navarro, M.-O. Benoit-Biancamano, J. Ronholm and S. George, *Nanomaterials*, 2022, **12**, 2179.
15 S. Majumder and S. George, in *Ayurvedic Herbal Preparations in Neurological Disorders*, ed. M. Muralidhara and P. S. Rajini, Academic Press, 2023, pp. 611–633.
16 G. Truchetti, E. Bouchard, L. Descôteaux, D. Scholl and J. P. Roy, *Can. J. Vet. Res.*, 2014, **78**, 31–37.
17 J. P. Roy, L. DesCôteaux, D. DuTremblay, F. Beaudry and J. Elsener, *Can. Vet. J.*, 2009, **50**, 1257–1262.
18 X. Villanueva, L. Zhen, J. N. Ares, T. Vackier, H. Lange, C. Crestini and H. P. Steenackers, *Front. Microbiol.*, 2023, **13**, 987164.
19 S. Nistorescu, G. G. Pircalabioru, A.-M. Udrea, Á. Simon, M. L. Pascu and M.-C. Chifiriuc, *Coatings*, 2020, **10**, 1230.
20 R. Kong, O.-H. Kang, Y.-S. Seo, S.-H. Mun, T. Zhou, D.-W. Shin and D.-Y. Kwon, *Asian Pac. J. Trop. Med.*, 2016, **9**, 542–546.
21 P. Yadav, A. B. Yadav, P. Gaur, V. Mishra, Z. I. Huma, N. Sharma and Y. O. Son, *Biomedicines*, 2022, **10**, 3282.
22 G. Tiwari, R. Tiwari and A. K. Rai, *J. Pharm. BioAllied Sci.*, 2010, **2**, 72–79.
23 C. Stein, O. Makarewicz, J. A. Bohnert, Y. Pfeifer, M. Kesselmeier, S. Hagel and M. W. Pletz, *PLoS One*, 2015, **10**, e0126479.
24 N. M. Soliman, F. Shakeel, N. Haq, F. K. Alanazi, S. Alshehri, M. Bayomi, A. S. M. Alenazi and I. A. Alsarra, *Molecules*, 2022, **27**, 4468.
25 L. Shao, S. Majumder, Z. Liu, K. Xu, R. Dai and S. George, *J. Photochem. Photobiol., B*, 2022, **231**, 112450.
26 J. M. Radziwill-Bienkowska, P. Talbot, J. B. J. Kamphuis, V. Robert, C. Cartier, I. Fourquaux, E. Lentzen, J.-N. Audinot, F. Jamme, M. Réfrégiers, J. K. Bardowski, P. Langella, M. Kowalczyk, E. Houdeau, M. Thomas and M. Mercier-Bonin, *Front. Microbiol.*, 2018, **9**, 794.
27 E. Brouillette, G. Grondin, C. Lefebvre, B. G. Talbot and F. Malouin, *Vet. Microbiol.*, 2004, **101**, 253–262.
28 E. Brouillette, G. Grondin, B. G. Talbot and F. Malouin, *Vet. Immunol. Immunopathol.*, 2005, **104**, 163–169.
29 S. Sana, S. Datta, D. Biswas and D. Sengupta, *Biochim. Biophys. Acta, Biomembr.*, 2018, **1860**, 579–585.
30 J. A. Sharp, C. Lefevre, A. J. Brennan and K. R. Nicholas, *J. Mammary Gland Biol. Neoplasia*, 2007, **12**, 47–58.
31 V. J. Stella, V. M. Rao, E. A. Zannou and V. Zia, *Adv. Drug Delivery Rev.*, 1999, **36**, 3–16.
32 Y. Herdiana, N. Wathoni, S. Shamsuddin and M. Muchtaridi, *Heliyon*, 2022, **8**, e08674.
33 H. Katas, Z. Hussain and T. C. Ling, *J. Nanomater.*, 2012, **2012**, 45–45.
34 J.-j. Kang, Y.-m. Liu, L.-l. Zhao, F. Xu, X.-j. Chen, X. Yan and X.-b. Li, *J. Integr. Agric.*, 2018, **17**, 1234–1240.
35 N. Ojkic, D. Serbanescu and S. Banerjee, *mBio*, 2022, **13**, e0065922.
36 S. George, I. Tay, W. H. Phue, H. Gardner and B. Sukumaran, *J. Biomed. Nanotechnol.*, 2019, **15**, 2216–2228.
37 A. J. Seukep, V. Kuete, L. Nahar, S. D. Sarker and M. Guo, *J. Pharm. Anal.*, 2020, **10**, 277–290.

38 A. Nasti, N. M. Zaki, P. De Leonardis, S. Ungphaiboon, P. Sansongsak, M. G. Rimoli and N. Tirelli, *Pharm. Res.*, 2009, **26**, 1918–1930.
39 N. M. Zaki, A. Nasti and N. Tirelli, *Macromol. Biosci.*, 2011, **11**, 1747–1760.
40 Á. Rusznyák, M. Malanga, É. Fenyvesi, L. Szente, J. Váradi, I. Bácskay, M. Vecsernyés, G. Vasvári, Á. Haimhoffer, P. Fehér, Z. Ujhelyi, B. Nagy Jr., Z. Fejes and F. Fenyvesi, *Pharmaceutics*, 2021, **13**, 157.
41 N. M. Zaki and M. M. Hafez, *AAPS PharmSciTech*, 2012, **13**, 411–421.
42 D. Sun, W. Gao, H. Hu and S. Zhou, *Acta Pharm. Sin. B*, 2022, **12**, 3049–3062.
43 E. Brouillette and F. Malouin, *Microbes Infect.*, 2005, **7**, 560–568.
44 Y. Chen, L. Tian, F. Yang, W. Tong, R. Jia, Y. Zou, L. Yin, L. Li, C. He, X. Liang, G. Ye, C. Lv, X. Song and Z. Yin, *Adv. Wound Care*, 2019, **8**, 341–354.
45 Z. Tong, W. He, X. Fan and A. Guo, *Front. Vet. Sci.*, 2022, **8**, 803657.
46 H. D. Jhundoo, T. Siefen, A. Liang, C. Schmidt, J. Lokhnauth, A. Béduneau, Y. Pellequer, C. C. Larsen and A. Lamprecht, *Pharmaceutics*, 2020, **12**, 1038.
47 S. L. Appleton, S. Navarro-Orcajada, F. J. Martínez-Navarro, F. Caldera, J. M. López-Nicolás, F. Trotta and A. Matencio, *Biomolecules*, 2021, **11**, 1384.